

# Thermal regeneration of activated carbon saturated with nitrate ions from an artisanal furnace

Horo Koné<sup>1</sup>, Konan Edmond Kouassi<sup>2</sup>, Affoué Tindo Sylvie Konan<sup>1</sup>, Kopoin Adouby<sup>1</sup>, Kouassi Benjamin Yao<sup>1</sup>

<sup>1</sup>Laboratoire des Procédés Industriels, de Synthèse de l'Environnement et des Energies Nouvelles (LAPISEN); Institut National Polytechnique Houphouët-Boigny, BP 1313 Yamoussoukro, Côte d'Ivoire

<sup>2</sup>Laboratoire de Thermodynamique et de Physico-Chimie du Milieu (LTPCM), UFR-SFA, Université Nangui-Abrégoua, 02 BP 801 Abidjan 01, Cote d'Ivoire

Received: 11 Oct 2020; Received in revised form: 06 Nov 2020; Accepted: 09 Nov 2020; Available online: 11 Nov 2020

©2020 The Author(s). Published by Infogain Publication. This is an open access article under the CC BY license

(<https://creativecommons.org/licenses/by/4.0/>).

**Abstract**— *The present study was initiated to help the simple and less expensive regeneration of activated carbons after saturation in rural area. In order to determine a regeneration time and the number of regeneration cycles, an adsorption test was necessary. Thus, 3h and 4 cycles of carbon regeneration are obtained after evaluation of the performance, percentage and adsorption capacity after each cycle. Regeneration percentages of 71.29, 54.05, 40.40, 28.06 % and 72.6, 69.84, 64.33, 34.98 % for respective concentrations of  $30 \pm 1.2$  mg/L and  $55 \pm 1.6$  mg/L are observed. Also, the performances of activated carbon 8.5, 10, 12, 20 g/L and capacities 24.04, 19.93, 14.9 and 10.35 mg/g 35.7, 34.12, 31.43 and 17.09 mg/g respectively for dry season and rainy season were necessary to fix the number of cycles. The artisanal furnace with its ease of installation and its maximum temperature of  $500 \pm 2^\circ\text{C}$  is suitable for the regeneration of saturated activated carbon.*

**Keywords**— *Regeneration, saturated activated carbon, artisanal furnace.*

## I. INTRODUCTION

Sustainable development necessarily involves recycling everything we use in order to guarantee the life for future generations. It is in this perspective that researchers have taken an interest in the regeneration of activated carbon in order to protect what the forerunners used in their productions. Several regeneration methods are available. It can be extractive using a volatile organic solvent [1], a fluid such as CO<sub>2</sub> [2] or concentrated solutions of surfactants [3], to extract the pollutants from the activated carbon. However, its implementation remains costly even if this opinion is not unanimous. Indeed, some estimates consider it much cheaper than thermal regeneration [4,5]. Regeneration can be done in the same way by vapour desorption with the use of temperatures between 105 and 140 °C [6] to just shift the adsorption equilibrium. Like the first mentioned, it is limited for

activated carbons having adsorbed volatile compounds. In addition to the two methods, thermal regeneration, which is the most common method, perfectly regenerates the activated carbon [7]. [8] reported percentages of 92-95% and 96-98% regeneration for carbons regenerated at 500°C. In addition, this method leads to a mass loss of coal in the order of 7-10%, and can reduce the porosity of the adsorbent [9]. Also, certain bacteria and enzymes are involved in the regeneration of activated carbons. In this way, bacteria or micro-organisms that can degrade the pollutant are brought into contact with the carbon [5]. This method is limited in the presence of poorly biodegradable pollutants or when concentration levels reach the inhibition or toxicity threshold [10]. Electrolytes can be used for electrochemical regeneration. [11] and [12] have used NaCl, Na<sub>2</sub>SO<sub>4</sub> or NaHCO<sub>3</sub> as electrolytes, respectively. [13] in using the electrochemical route, have reported a regeneration percentage ranging from 70 to 90%

using diclofenac. However, [5] noted that the choice of NaCl electrolyte gives better results but remains limited due to the production of toxic organochlorine compounds generated. Overall, all of these methods are expensive. Indeed, [13] reported a total consumption of 3.80 kWh kgGAC-1 during the chemical regeneration of coal. In view of the additional costs associated with coal regeneration, an adaptation of one of the methods in rural areas is the objective of this study. The originality of this work lies in the use of an artisanal furnace especially for the regeneration of activated carbon saturated. Indeed, most research is focused on the production of activated carbon at lower cost in rural areas but few studies have focused on simplified and practicable regeneration in rural areas. Thus, the thermal regeneration method will be applied and the electric furnace will be replaced by a small-scale furnace that is easily feasible in rural areas.

## II. METHODOLOGY

### 2.1 Presentation of the artisanal oven

The artisanal furnace was built on the northern site of the INP-HB (Figure 4). Several materials were used in its construction. The main materials were clay, banco bricks and a metal skeleton Fig. 1A. Unlike the modern kiln the artisanal furnace was built around two chambers. The feed chamber, rectangular in shape and with a volume of 15000 cm<sup>3</sup>, was created to facilitate the supply of firewood to the kiln, which was the source of energy to operate it. As for the pyrolysis chamber in conical form and with a volume of 100480 cm<sup>3</sup>, it received the material to be carbonized. The two chambers were separated by a metal plate. In order to obtain hermetic conditions during carbonization Fig. 1B, the pyrolysis chamber was equipped with a closure.

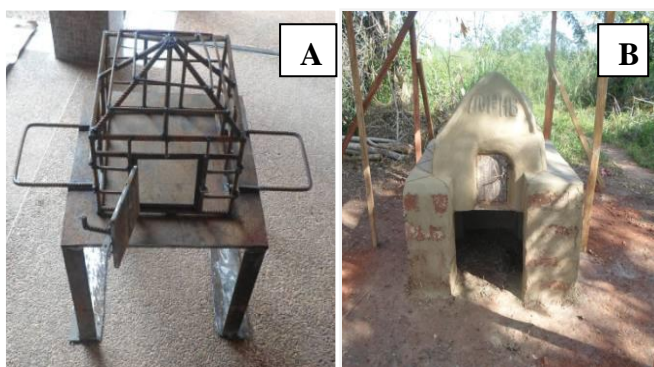


Fig. 1: Skeleton of the traditional oven (A) and the traditional oven (B)

### 2.2 Temperature evaluation

First, the oven temperatures were determined using a thermometer in time steps of 30min to 210 min. Then, from 210 min the time steps were varied from 15 min to 255 min or it became 20 min. Finally, the maximum temperature of the oven was determined by constructing the temperature versus time diagram.

### 2.3 Characterization of raw *Borassus aethiopicum* activated carbon (BA-AC)

#### 2.3.1 Mineralogical composition

The mineralogical composition of the BA-AC concerned the level of carbon, nitrogen and hydrogen. This was concerned C, H, and N in solid Biocombustibles. As the BA-AC were not pre-dried, the moisture content was determined and calculations were made on the gross basis of the expressions below.

$$C_{\text{sec}} = C_{\text{brut}} \times 100 / (100 - T_{\text{hum}})$$

$$N_{\text{sec}} = N_{\text{brut}} \times 100 / (100 - T_{\text{hum}})$$

$$H_{\text{sec}} = (H_{\text{brut}} - 0,1119 \times T_{\text{hum}}) \times 100 / (100 - T_{\text{hum}})$$

Whith C is Carbon content, N indicate Nitrogen content, H the Hydrogen content and T<sub>hum</sub> represent moisture content of the sample

For the percentage of oxygen contained in *Borassus aethiopicum* activated carbon was evaluated according to the Equation 1 [14].

$$\%O = 100 - \%C - \%N - \%ash \quad (1)$$

#### 2.3.2. Determination of BA-AC texture

The textural determination of carbon led to the Nitrogen adsorption experiment at a temperature of 77K to 25 °C. To do this, a BET meter was used (Quantachrome Novamix version 11.03). Considering an initial pressure p<sub>0</sub>, increasing pressure values were applied which allowed the corresponding equilibrium pressure p to be determined. At each applied pressure value, a volume V of gas was adsorbed. The adsorption isotherm was obtained by constructing the function V(ads) = f(p/p<sub>0</sub>).

Where V(ads) was the volume of gas adsorbed and p/p<sub>0</sub> the ratio of the pressure

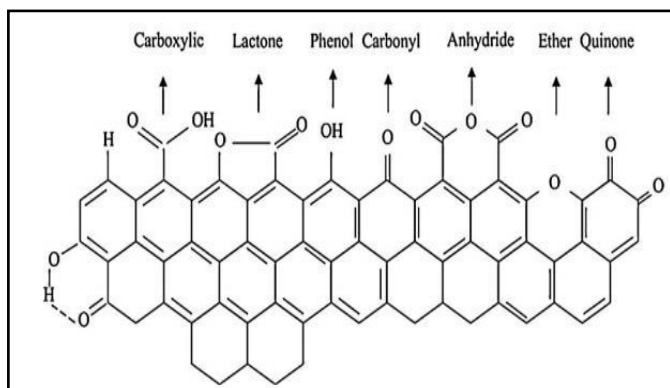
Considering the adsorption isotherms, the BET surface area was calculated using the equation 2

$$S_{\text{BET}} = \frac{V_m \times N_A \times a_m}{m \times V_M} \quad (2)$$

Where S<sub>BET</sub> is the specific surface area (m<sup>2</sup>/g), N (A) is the Avogadro number, a<sub>m</sub> indicates the surface area occupied by the N<sub>2</sub> molecule (0.1627 nm<sup>2</sup>/molecule of nitrogen), m is the mass of the sample (g) and V<sub>M</sub> is the molar volume of N<sub>2</sub> at TPN (22414 cm<sup>3</sup>/mole).

### 2.3.3 Activated carbon surface chemistry

The chemical functions on the surface of the coal were determined using infrared spectroscopy to obtain the spectrum shown in Fig. 3. Referring to the different functional groupings on the coal surface a structure with acidic groupings was proposed by [15] (Fig. 2). Based on



this structure, the BA-AC structure has been proposed [15].

Fig. 2 : Fonction acide à la surface du charbon

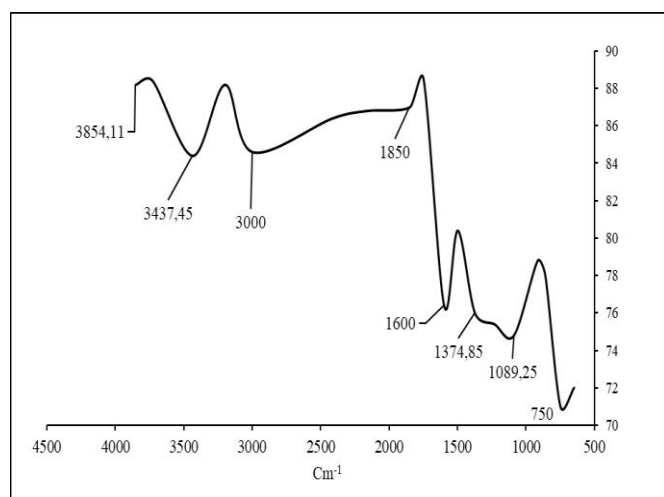


Fig. 3: Fourier infrared spectrum to be transformed

### 2.3.4 pH at zero load point

The pH at zero load was determined using the following methodology. First, 10 Erlenmeyer flasks containing 50 mL of distilled water were selected. Then, initial pH values (pHi) ranging from 2 to 12 were selected after adjustment with hydrogen chloride (0.1M) or sodium hydroxide (0.1M) solutions. To each Erlenmeyer flask, 50 mg of activated carbon was added. Then the whole was stirred for 24 h at room temperature. Finally, the new pH values were determined after 24 hours of stirring. The pH of zero charge was obtained when pHi= pHf (Konan et al., 2019).

### 2.4 Determining the regeneration time

The regeneration time required for saturated carbon was tested in the laboratory. First, 300 g of saturated activated carbon with nitrate ions was divided into 5 samples of 60 g. Then, each 60 g sample placed in a hermetically sealed container was heated in the oven at  $500 \pm 1.15$  °C for times ranging from 1h to 5h. Finally, each sample formed a column that allowed a nitrate adsorption test to be performed on two samples with different concentrations of  $30 \pm 1.2$  mg/L and  $55 \pm 1.6$  mg/L determined previously in raw lakes water respectively in dry season and rainy season. The adsorption capacities and performances of the different regenerated carbons were determined according to equations 3 and 4, respectively [16].

$$N_0 = \frac{A_i}{m} \int_0^{V_a} \left(1 - \frac{A_t}{A_0}\right) dv \quad (3)$$

$$ARE = \frac{\text{Masse of adsorbent(g)}}{V_b(L)} \quad (4)$$

Were  $N_0$  is adsorption capacities,  $V_b$  is the volume of water treated before the breakthrough point and AER is adsorbent exhaustion rate.

### 2.5 Number of regeneration cycles

Since activated carbon regeneration is not eternal, the number of regeneration cycles was further tested in laboratory. The carbon was regenerated by applying the conditions of the column that gave the best adsorption capacity when determining the regeneration time. A total of four regeneration cycles (R1, R2, R3 and R4) were carried out. The different adsorption capacities and performance of the columns after each regeneration were determined according to equations 3 and 4.

### 2.6 Evaluation of the regeneration percentage

The following method has been adopted. First, the adsorption capacity of the raw activated carbon was determined. Then the adsorption capacity of the regenerated carbon was determined. Finally, the regeneration percentages were calculated according to equation (5) [13,17].

$$\%RE = \frac{q_r}{q_c} \times 100 \quad (5)$$

where %RE is the percentage of regeneration,  $q_r$  is the adsorption capacity of the regenerated carbon and  $q_c$  is the adsorption capacity of the raw activated carbon.

### 2.7 Evaluation of carbon loss after regeneration

First, 50 g of coal was weighed and then placed in a container with a mass  $m_0$ . The container was then placed in an artisanal furnace at a temperature of  $500 \pm 1.15$  °C.

Finally, after 3 hours of regeneration, the container was removed and weighed with its contents. The loss of carbon was calculated according to equation (6).

$$\%P = \frac{m_i - m_f}{m_i} \times 100 \quad (6)$$

2.8 Study of column breakthrough after regeneration

The regenerated charcoal was tested by continuous adsorption of a raw lake water. Two nitrate concentrations were used ( $C_0=30 \pm 1.2$  mg/L;  $C_0=55 \pm 1.6$  mg/L). This water was used on the one hand to determine the regeneration time and on the other hand to determine the number of regeneration cycles. The logistic model indicated by equation (7) was used to determine the volumes treated at the breakthrough point  $t_{50}$ .

$$\ln\left(\frac{C_t}{C_0 - C_t}\right) = k(t - t_{50}) \quad (7)$$

With  $C_0$ : Initial concentration;  $C_t$ : concentration at a given instant and  $t_{50}$  the breakthrough time

2.9 Testing activated carbon on lake water to remove turbidity after regeneration

Filters were designed and then combined in series of 3,6 and 9. All filters in a series were identical. Their characteristics are shown in Table 1 and fig. 4. The filters were mounted on a device installed at Lac Dougba in Ivory coast to conduct the tests on recycled activated carbon. For each series of columns turbidity elimination tests in the lake water were carried out after each regeneration over two dry season.

Table. 1: Filter characteristics

Characteristics	Dimensions
Outside diameter	22,5 cm
Inner diameter	20cm
Height	44.7 cm
Empty column volume	14035,8 cm <sup>3</sup>
Volume of coarse sand	1884 cm <sup>3</sup>
Volume of coal	7850 cm <sup>3</sup>
Volume of fine sand	1256 cm <sup>3</sup>

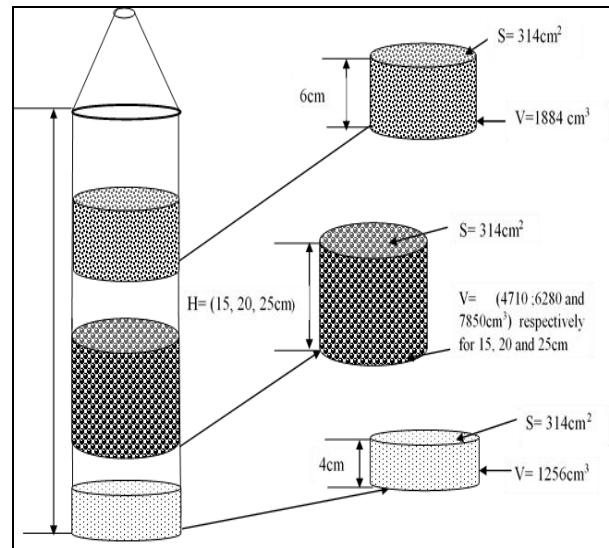


Fig. 4: Colonne test for turbidity removal

III. RESULTS

3.1 Assessment of artisanal oven temperature

From Fig. 5, it can be seen that the heating temperatures of the furnace vary over time. When the furnace is fed, it gradually heats up and then reaches its maximum temperature of 500.67 °C, which remains constant for 30 min, regardless of the feed supplied to the furnace. Like the heating, the cooling of the furnace is gradual. In view of the maximum temperature obtained, this furnace can be used for the regeneration of certain saturated activated carbons. Indeed, compared to the studies of [8,18], this furnace can be used for the regeneration of some saturated activated carbons. which respectively varied the temperatures from 250 to 450 °C and 20 to 600 °C from modern furnaces in order to remove the dyes adsorbed by the coal, the artisanal furnace could replace the modern furnace. It will be limited only if the absorbed pollutant requires a destruction temperature higher than the maximum temperature of 500 °C.

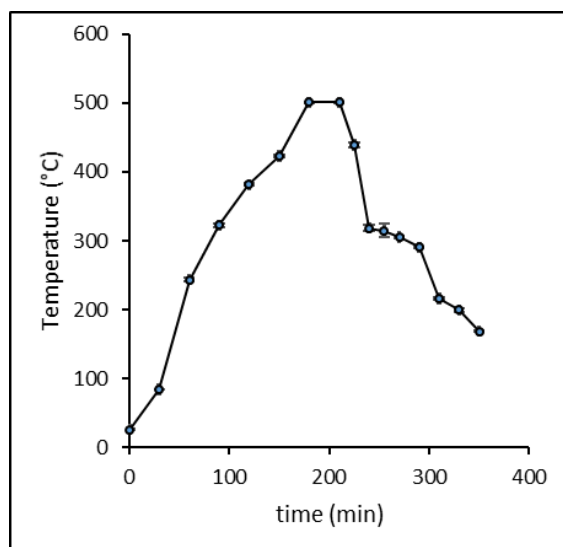


Fig. 5: Determination of the temperature of the artisanal furnace in operation

### 3.2 Some characteristics of raw BA-AC

#### 3.2.1. Elemental composition of activated carbon

The elemental analysis of the activated charcoal prepared in a traditional oven was carried out taking into account four compounds (table 3). These were carbon, nitrogen, hydrogen and oxygen. Indeed, this analysis reveals that the carbon is made up of 74 % carbon, 2.77 % hydrogen, 0.69 % nitrogen and 19.48 % oxygen. However, the percentage of 74 % carbon obtained shows that the roast wood is rich in carbon and suitable for the production of quality activated carbon [18]. This carbon percentage falls well within the range [50; 90 %] recognized by [19,20] as a means of judging the quality of a plant to produce activated carbon. Indeed, these authors believe that the carbon content of a plant must be in the range [50; 90 %] for it to be eligible for the production of activated carbon. In addition, this percentage is well above those found by [14] which are 33.48 % and 37.43 % respectively for peanut shells and coconut shells. The branches of *Borassus aethiopum* (BA) are therefore suitable for the production of quality activated carbon.

Table. 2: Elemental composition of *Borassus aethiopum* activated carbon

Elements	Percentage (%)
N	0.69
C	74
H	2.77
O	19.48

#### 3.2.2 Pore distribution and BET surface

Raw activated carbon before saturation and saturated activated carbon were characterized. The characteristics are listed in the table 3 below. Analysis of the table shows that the specific surface area of coal decreases when it is saturated. Indeed, the specific surface area of 1431.61 m<sup>2</sup>/g has increased to 83.58m<sup>2</sup>/g after saturation. This decrease is simply due to the closure of the pores of the carbon by the adsorbed pollutants. This finding is consistent with that of [8]. These authors found that after saturation of the carbon by BB9, the specific surface area decreased from 1131 m<sup>2</sup>/g to 679 m<sup>2</sup>/g. However, the saturated activated carbon is still microporous with an ash content of 12.58 % and a pHzc of 5.46. This high ash content could be linked to the deterioration of part of the carbon following the high temperature applied to calcine the pollutants adsorbed by the activated carbon. Also, the increase of the pHzc could be induced by the ashes of the pollutants calcined during regeneration. In addition, the ash of the regenerated carbon is a mixture of part of the activated carbon and the adsorbed pollutants. This finding on the transformation of part of the carbon into ash corroborates [21] assertion. He showed that regeneration makes the carbon friable due to the regeneration temperature which degrades part of the carbon into ash. The curves of adsorption/desorption of N<sub>2</sub> from raw and regenerated carbon are shown respectively in fig.6 and fig. 7. The shape of the two curves shows that the regenerated activated carbon is always microporous and mesoporous if we stick to the classification of IUPAC which is type IV.

Table. 3: Characteristics of the raw activated carbon before saturation

Parameters	BA-AC values	BA-AC regeneration values
SBET(m <sup>2</sup> /g)	1431.61	83.58
SEX(m <sup>2</sup> /g)	1432	85
Vp(nm)	1.85	1.849
Vt(nm)	0.971	4.844
Vmicr(nm)	0.279	0.199
Ash%	2.89	12.58
pHzc	5	5.46

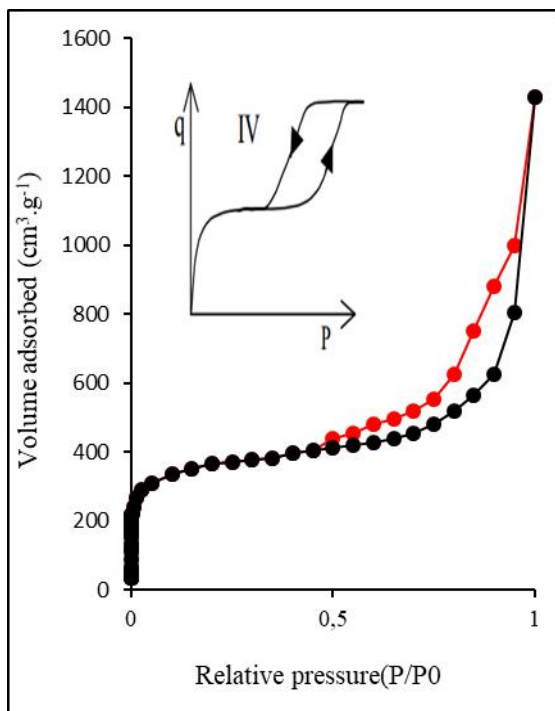


Fig. 6: Adsorption and desorption curve of raw BA-BC

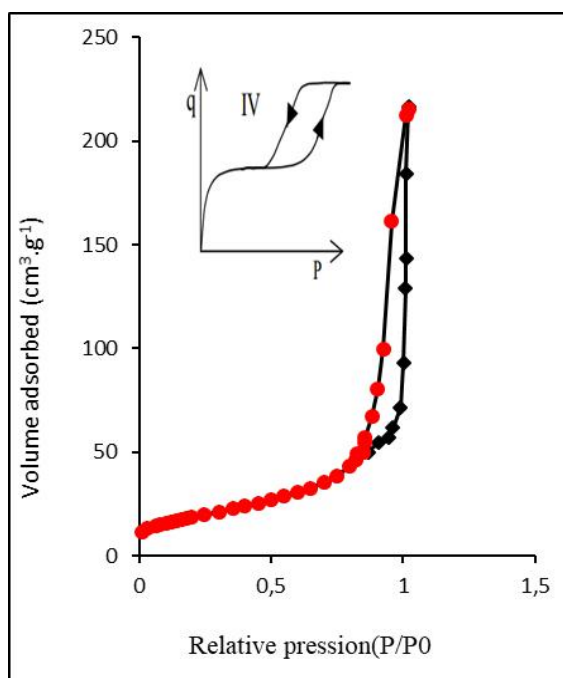


Fig.7: Adsorption and desorption curve of saturated activated carbon from BA-BC

### 3.2.3 BA-AC chemical surface

The analysis of the infrared spectrum provided the information shown in table 1. Borassus aethiopum activated carbon (BA-AC) contains O-H functional groups corresponding to the 723cm<sup>-1</sup> and 750cm<sup>-1</sup> elongation

vibrations. So, referring to the claims of [22-23], the possible chemical compounds would be the aromatic compounds. As for the C-H functional group, it appeared at wavelengths 1200 cm<sup>-1</sup> and 3000 cm<sup>-1</sup>. Then in agreement with [15-24], the possible chemical compounds are quinones. Also, chemical compounds such as carboxylic acids and esters are present. This presence is deduced from the presence of C=O functional groups detected at 1300, 3500-4000 cm<sup>-1</sup> and 1600-1800 cm<sup>-1</sup> elongation vibrations in agreement with [15-25]. Finally, at intervals of 1330-1530 cm<sup>-1</sup> and 1000-1220 cm<sup>-1</sup> indicating the presence of N-H and C-OH functional groups respectively. Thus, according to [15], nitro groups and phenolic groups are present. All functional groups detected are summaries in table 3. Referring to the structure proposed by [15] and the functional groupings found on the surface of the BA-AC, a possible structure of the BA-AC is proposed Fig. 8.

Table. 4: Functional groups and chemical compounds

Elongation vibrations (cm-1)	Functional groupings	Possible chemical compounds
723, 750	O-H	Aromatic compounds
1200 ; 3000	C-H	Quinones
1300 ; 3500-4000	C=O	Esters
1600-1800 ;	C=O	Carboxylic acids
1330-1530	N-H	Nitro group
1000-1220	C-OH	Phenolic groups

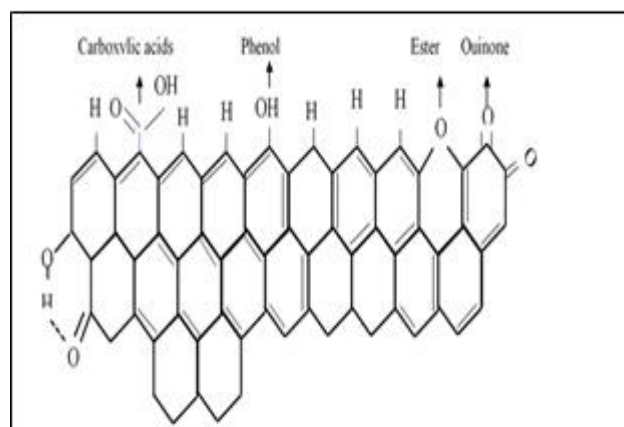


Fig. 8: possible structure of BA-AC with acids groups

### 3.2.4 Crystalline form of activated carbon

The Raman spectrum fig. 9 is used to determine the degree of crystallization of the material. In general, two peaks D and G appear on the Raman spectrum. The G peak, which expresses the graphite content, and the D peak, which expresses the diamond content, appear respectively at wavelengths between  $1350\text{-}1355\text{ cm}^{-1}$  and  $1570\text{-}1585\text{ cm}^{-1}$  [26]. According to [26-27] it is possible to know the textural property of a coal by making the  $I_D/I_G$  ratio. In this study, the Raman spectrum shown in Figure 2 has two peaks. The first peak D appeared at wavelength  $1348.99\text{ cm}^{-1}$  with intensity 8566.19 a.u. and the second peak appeared at wavelength  $1591.21\text{ cm}^{-1}$  with intensity 9342.15 a.u. By determining the coefficient of the  $I_D/I_G$  ratio the value of 0.917 is obtained. According to [28,29] a high  $I_D/I_G$  ratio value implies an organized male carbon structure and a defective activated carbon. Then according to [26] which obtained  $I_D/I_G$  ratios ranging from 0.55 to 0.70, *Borassus aethiopum* carbon has high graphitization [30-31]. Also, the G peak obtained at the wavelength of  $1591.27\text{ cm}^{-1}$  as noted by [32], the coal has an ordered structure.

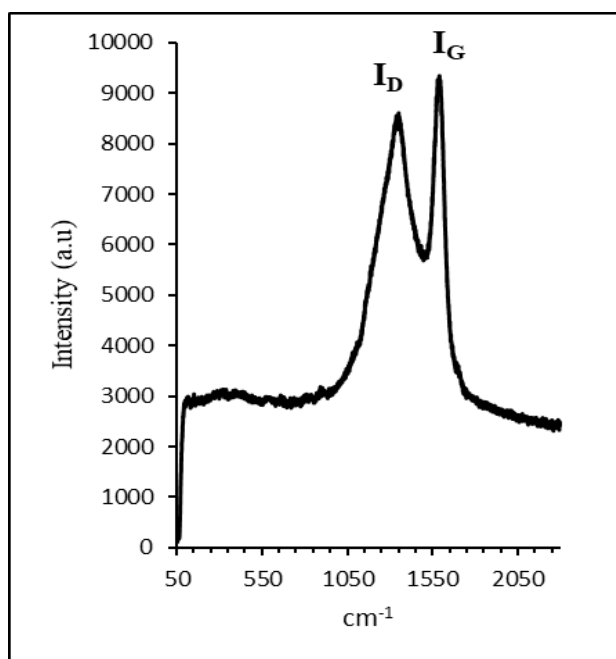


Fig. 9: Raman spectrum of BA-AC

### 3.2.5. Diffraction du charbon actif BA-AC

The diffraction of *Borassus aethiopum* carbon activated with copper sulfate resulted in Fig. 10. Observing the diffractogram, one finds  $\text{Cu}_1.8\text{S}$  digenite and tenorite ( $\text{CuO}$ ). The presence of these two elements in the coal makes it possible to understand that, despite the fact that the washing water of the coal gave zero values to

the atomic absorption spectrometer, copper is present in the coal. The presence of digenite and tenorite are related to the copper present in the copper sulphate solution used to impregnate the activated carbon. Indeed, during activation the heated copper gives tenorite ( $\text{CuO}$ ) of which digenite ( $\text{Cu}_1.8\text{S}$ ) is the intermediate step. This finding corroborates that of [33] who obtained copper oxide ( $\text{CuO}$ ) nanostructures by heating metallic copper.

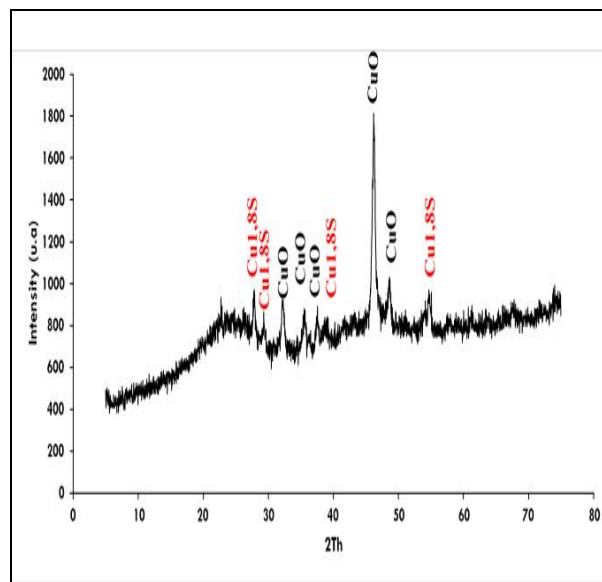


Fig. 10: Spectre of BA-AC XRD

### 3. 3 Regeneration time

In order to retain the residence time required for BA-AC in the furnace in order to acquire a good part of its adsorbent power the fig. 11 A and Fig. 11 B are obtained. To ensure the effectiveness of regeneration, a nitrate adsorption test in synthetic solution was used to determine the adsorption capacities and performance of the regenerated activated carbon at different times. As mentioned [16], between two activated carbons, the best performing one has the lowest AER value. Therefore, by comparing the adsorbent exhaustion rate (AER) 20, 12, 8.5, 12 and 15 of the carbons at the respective regeneration times of 1h, 2h, 3h, 4h and 5h, and the different adsorption capacities, 3h was selected. Figure 11 A shows that the AERs decreased steadily with increasing time to reach a minimum of  $8.57\text{ g/L}$  from three hours' regeneration time before gradually increasing to reach  $15\text{ g/L}$  at a regeneration time of 5h. Also, the adsorption capacities which are  $8.56$ ,  $15.6$ ,  $19.15$ ,  $14.83$  and  $10.53\text{ mg/g}$  for  $C_0=30\pm 1.2\text{ mg/L}$  as initial concentration and  $20.43$ ,  $32.05$ ,  $35.47$ ,  $27.06$  and  $23.95\text{ mg/g}$  for  $C_0=55\pm 1.6\text{ mg/L}$  corresponding respectively to times 1, 2, 3, 4, and 5 h. In view of the AER and adsorption capacities which are

better at the 3h regeneration time, this time was chosen as the appropriate time for the whole study.

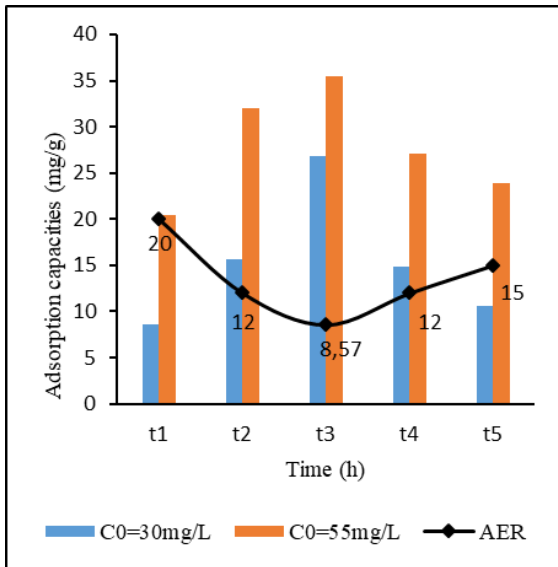


Fig. 11A: Comparative development of each AER adsorption capacities during the determination of the regeneration time

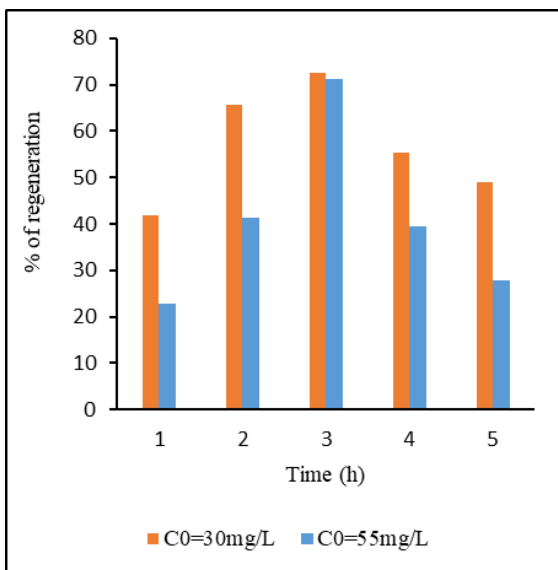


Fig. 11B: Comparative regeneration percentage during the determination of the regeneration time during the determination of the regeneration time

### 3.4 Number of regeneration cycles

Table 5A and table 5B show the evolution of the adsorption capacities and the AERs obtained after each regeneration cycle and figs (12A and 12B) show respectively the regeneration adsorptions capacities and regeneration percentages. According to Table V and Figure 9 the adsorbent exhaustion rate (AER) increase while the adsorption capacities gradually decrease from

the first regeneration cycle to the fourth regeneration cycle. Adsorbent exhaustion rate (AER) values of 8.5, 10, 12 and 20 respectively for regeneration cycles 1,2,3 and 4 were obtained. This loss of performance of the carbon after each regeneration results in a loss of adsorption capacity of 24.04, 19.93, 14.9 and 10.35 mg/g for dry season (30± 1.2 mg/L) and 35.7, 34.12, 31.43 and 17.09 mg/g for rainy season (55 ± 1.6 mg/L). The table. 4 and figures 13 show that the AER and adsorption capacities are in the opposite order. [16,34] made similar remarks. In addition,[34] reported capacities of 2.9 10<sup>6</sup> and 3.34 10<sup>6</sup> for AERs of 2.1 and 1.8 respectively. As for [16], they obtained adsorption capacities of 3.72, 4.64 and 4.79 against EARs of 2.7, 2.1 and 2 respectively. This decrease in capacity was noted by [13]. In addition, [13,21] showed that activated carbon loses its adsorptive capacity during regeneration. Thus, [13] proposed a maximum of 5 regenerations. Activated carbon losses ranged from 9.54 % to 23.58 % in the search for regeneration time. In the phase of determining the number of regeneration cycles, activated carbon losses varied from 8 % to 17.02 %. The general observation is that Activated carbon losses increase with the number of regeneration cycles and the length of residence time. These losses are generally beyond the loss range set by [7] which is 7 to 10 % when using a modern furnace. These losses over the regeneration cycles would be related to the use of an artisanal furnace and to a deterioration of the activated carbon over the regeneration cycles. Indeed, [21] showed that activated carbon becomes more friable more it is regenerated. Therefore, he recommends that the number of regeneration cycles at less than 5.

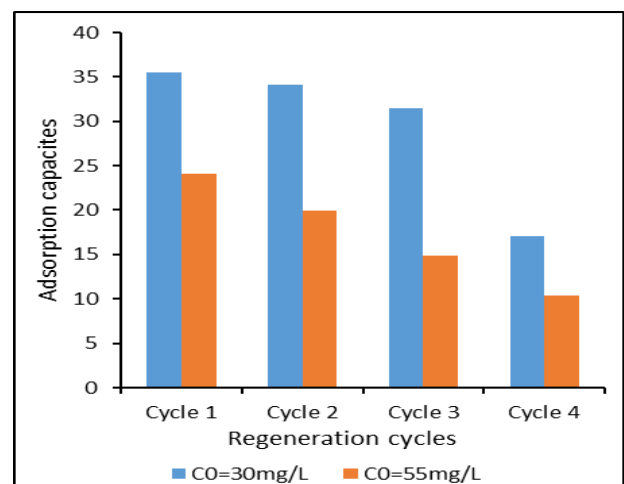


Fig. 12A: Variation of adsorption capacity as a function of regeneration cycles

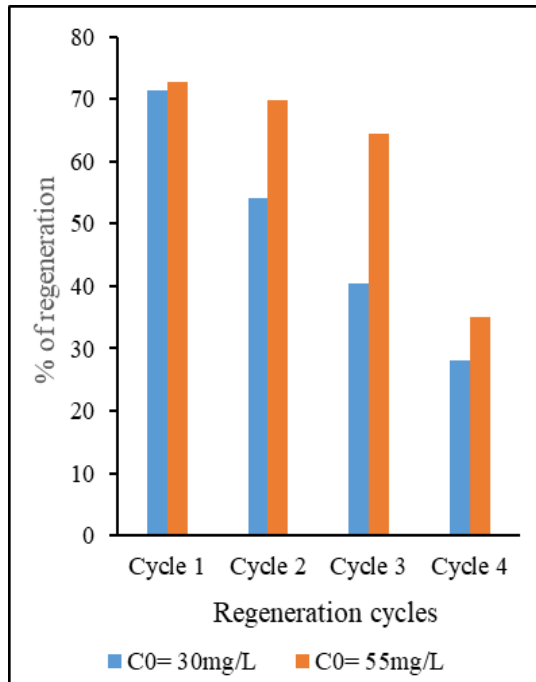


Fig. 12B: Variation of regeneration efficient as a function of regeneration cycles

Table. 5: Characteristics of regeneration times and regeneration cycles (dry season)

C <sub>0</sub> =30 ± 1.2 mg/L	
T(h)	BA-AC Q(mg/g) R %R
1	8.56 31.87
2	15.6 58.10
3	26.86 71.29
4	14.83 55.21
5	10.53 39.20
Regeneration cycles	
1	24.04 71.29
2	26.87 54.05
3	14.9 40.40
4	10.35 28.06

Table. 6: Characteristics of regeneration times and regeneration cycles (rainy season)

C <sub>0</sub> =55± 1.6 mg/L				Loss
BA-AC Q(mg/g)	Q (mg/g) R	%R	AER (g/L)	%P
	20.43	41.81	20	9.54
	32.05	65.61	12	13.02
48.86	35.47	72.6	8.5	15
	27.06	55.39	12	22
	23.95	63.81	15	23.58
Regeneration cycles				
	35.47	72.6	8.5	8
48.86	34.12	69.84	10	10.44
	31.43	64.33	12	13.55
	17.09	34.98	20	17.02

3. 5 Breakthrough characteristics of the logistic model

Continuous adsorption of nitrate after regeneration gave the characteristics shown in the table5 and breakthrough curve for two different concentrations. For an initial concentration of 30 ± 1.2 mg/L, breakthrough times of 76.11, 67.103, 58.66 and 42.68 min were obtained for cycles 1, 2, 3 and the fourth regeneration cycle, respectively. When initial concentration was 55± 1.6 mg/L, breakthrough times 61.51, 56.421, 48.717 and 37.724 min are obtained for regeneration cycles 1, 2, 3 and 4 respectively. This decrease in breakthrough times

over the regeneration cycles reflects a decrease in the adsorbent capacity of the activated carbon. This loss of adsorption power over the regeneration cycles was evoked by [13] through the decrease in the regeneration percentages. In addition, the observation relating to the influence of concentration has attracted the attention of several researchers. [16] obtained breakthrough times of 920 and 484.1 min respectively for concentrations of 10 mg/L and 20 mg/L. Also, [34] obtained breakthrough times of 2479 and 1774 min respectively for initial concentrations of 16000 CFU/mL and 65000 CFU/mL. Similarly, [36] and [37] found that concentration has a negative impact on breakthrough times. Indeed, the breakthrough times 6395.3 min and 2252.7 min are obtained respectively for concentrations of 30 and 50mg/L by [36] during their study relating to the adsorption on fixed column of polycyclic aromatic hydrocarbons contained in wastewater. As for [37], breakthrough times

of 140 and 115 min corresponding respectively to concentrations of 20 and 30 mg/L of hexavalent chromium contained in wastewater.

Table. 7: Logistic parameters

[NO <sub>3</sub> <sup>-</sup> ] ]	Q (mL/min)	Cycles	K	t <sub>50</sub>	V(ml)	R <sup>2</sup>
30± 1.2 mg/L	20	1	0.071	76.11	1400	0.87
		2	0.072	67.10	1200	0.97
		3	0.062	58.66	1000	0.99
		4	0.070	42.68	600	0.99
55± 1.6 mg/L	20	1	0.07	61.51	1200	0.99
		2	0.061	56.42	1000	0.97
		3	0.071	48.72	800	0.99
		4	0.083	37.72	600	0.96

2.6 Application of regenerated activated carbon for removing turbidity in lake water

The series of filters used to test the coals after each regeneration (R1, R2, R3, R4) yielded the breakthrough curves in fig. 13, fig. 14 and fig. 15 for the series of 3, 6 and 9 filters respectively. Indeed, during the test, the filter is considered to be pierced if the C/C0=0.1 which is the ratio of the turbidity at the outlet of the filter to the initial turbidity. Considering the series of 3 filters and the volume of water treated at the point of breakthrough, volumes of 18, 10, 6, 4 and 2 m<sup>3</sup> of water are freed from their turbid state by passing respectively for the raw activated carbon, the first regeneration, the second, third and fourth regeneration. Similarly, with the series of 6 filters, the volumes obtained are 32 m<sup>3</sup> for the raw activated carbon, 28 m<sup>3</sup> for the first regeneration, 16m<sup>3</sup> for the second, 12 m<sup>3</sup> for the third and 6 cm<sup>3</sup> for the fourth regeneration. As for the series of 9 filters, volumes of 72, 42, 36, 30 and 22 m<sup>3</sup> with a turbidity in the filter water of less than 1 NTU starting from the raw activated carbon at the fourth regeneration. In view of these volumes, which decrease with the regeneration of the carbon, this confirms the comments of [21] who believes that the number of regenerations, especially thermal regeneration, should be less than 5. Also, with percentages of 100 % removal of the turbidity obtained, filters with three materials (coarse sand - granular activated carbon - fine sand) are more efficient than filters with a single activated carbon and those made up of two materials (sand and carbon). Indeed, [38] could only obtain 65 % reduction in turbidity with an activated carbon filter alone. As for [39], they were

obtained percentages ranging from 75 to 78 % by associating a layer of sand with carbon.

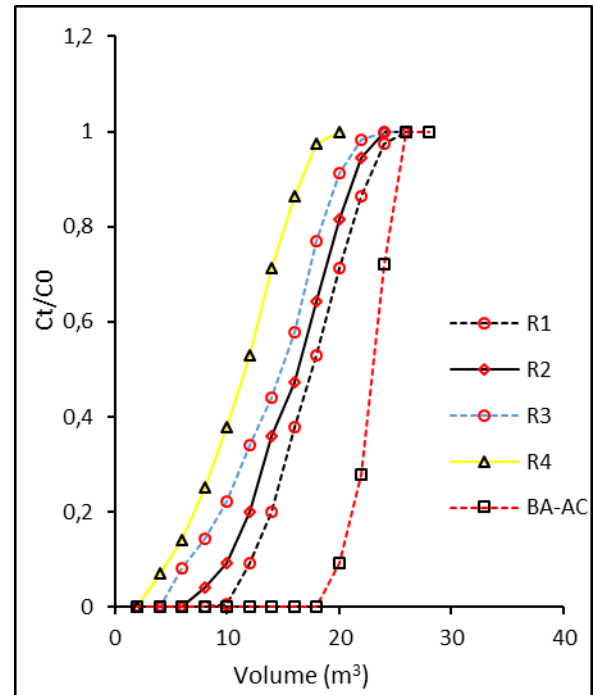


Fig. 13: Breakthrough curves of 9 columns at turbidity removal (turbidity=7,83 NTU ± 0,4; pH 6,49 ±0,2)

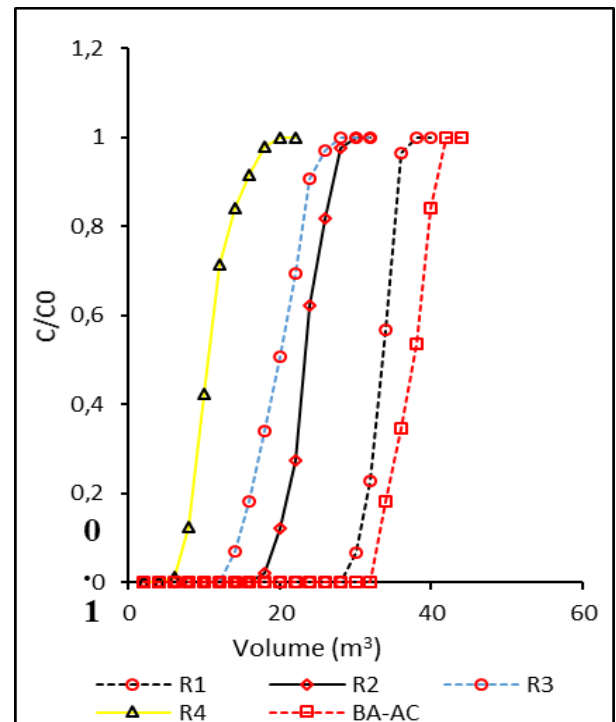


Fig. 14: Breakthrough curves of 6 columns at turbidity removal (7,83 NTU ± 0,4 ; pH 6,49 ±0,2)

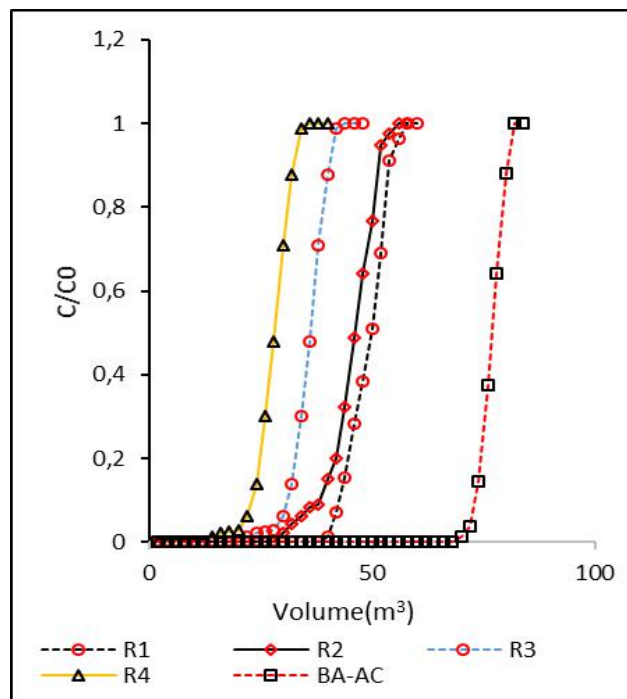


Fig. 15: Breakthrough curves of 9 columns at turbidity removal (turbidity =7,83 NTU  $\pm$  0,4; pH 6,49  $\pm$ 0,2)

#### IV. CONCLUSION

The adsorbent exhaustion rate (AER) 20, 12, 8.5, 12 and 15 g/L of the activated carbon at the respective times of 1h, 2h, 3h, 4h and 5h as well as the adsorption capacities of 8.56, 15.6, 19.15, 14.83 and 10.53 mg/g for  $C_0=30\text{mg/L}$  then 20.43, 32.05, 35.47, 27.06 and 23.95 mg/g for  $C_0=55\text{ mg/L}$  made it possible to fix the time of 3h as the necessary regeneration time. 4 regeneration cycles are obtained after evaluation of AERs 8.5, 10, 12, 20 and adsorption capacities 24.04, 19.93, 14.9 and 10.35 mg/L for dry season (30 mg/L) and 35.7, 34.12, 31.43 and 17.09 mg/L for rainy season (55mg/L). The four columns tested during the regeneration cycles gave breakthrough times 76.11, 67.103, 58.66 and 42.679min for  $C=30\text{mg/L}$  and 61.51, 56.421, 48.717 and 37.724 min for  $C=55\text{mg/L}$  according to the logistic model. In view of the regeneration percentages during the regeneration cycles, which are 71.29, 54.05, 40.40, 28.06 % and 72.6, 69.84, 64.33, 34.98 % respectively for dry season (30 mg/L) and rainy season (55 mg/L), the regeneration cycles deteriorate the quality of the activated carbon if they are prolonged. It can therefore be said that the artisanal furnace is a means of prolonging the use of activated carbon. However, for activated carbon that have adsorbed pollutants requiring high calcination temperatures above 500 °C, the traditional kiln will be inefficient because of its temperature limit of 500 °C.

#### ACKNOWLEDGMENT

The authors thank Mr David English PhD student, for reading and correcting the manuscript, thus contributing to improve the paper quality.

#### REFERENCES

- [1] Ferro-Garcia M, Utrera-Hidalgo E, Rivera-Utrilla J, Moreno-Castilla C and Joly J 1993 Regeneration of activated carbons exhausted with chlorophenols *Carbon* **31** 857–63
- [2] Madras G, Erkey C and Akgerman A 1993 Supercritical fluid regeneration of activated carbon loaded with heavy molecular weight organics *Industrial & engineering chemistry research* **32** 1163–8
- [3] Purkait M, Gusain D, DasGupta S and De S 2005 Adsorption behavior of chrysoidine dye on activated charcoal and its regeneration characteristics by using different surfactants *Separation science and technology* **39** 2419–40
- [4] Chihara K, Oomori K, Oono T and Mochizuki Y 1997 Supercritical CO<sub>2</sub> regeneration of activated carbon loaded with organic adsorbates *Water science and technology* **35** 261–8
- [5] Zanella O, Krummenauer Haro N, Cristina Tessaro I and Amaral Féris L 2015 Successive cycles of sorption/regeneration for granular activated carbon in the removal of nitrate ions *Desalination and Water Treatment* **55** 1908–14
- [6] le Cloirec P 2003 *Adsorption en Traitement de l'air* (Ed. Techniques Ingénieur)
- [7] Han X, Loggins V, Zeng Z, Favro L and Thomas R 2004 Mechanical model for the generation of acoustic chaos in sonic infrared imaging *Applied physics letters* **85** 1332–4
- [8] Durán-Jiménez G, Stevens L A, Hodgins G R, Uguna J, Ryan J, Binner E R and Robinson J P 2019 Fast regeneration of activated carbons saturated with textile dyes: Textural, thermal and dielectric characterization *Chemical Engineering Journal* **378** 121774
- [9] Han X, Wishart E and Zheng Y 2014 A comparison of three methods to regenerate activated carbon saturated by diesel fuels *The Canadian Journal of Chemical Engineering* **92** 884–91
- [10] Xiaojian Z, Zhansheng W and Xiasheng G 1991 Simple combination of biodegradation and carbon adsorption—the mechanism of the biological activated carbon process *Water Research* **25** 165–72
- [11] Zhang T, Walawender W P, Fan L, Fan M, Dugaard D and Brown R 2004 Preparation of activated carbon from forest and agricultural residues through CO<sub>2</sub> activation *Chemical Engineering Journal* **105** 53–9
- [12] Narbaitz R M and Cen J 1994 Electrochemical regeneration of granular activated carbon *Water Research* **28** 1771–8
- [13] Solano-Rivera V, Geris J, Granados-Bolaños S, Brenes-Cambronero L, Artavia-Rodríguez G, Sánchez-Murillo R

- and Birkel C 2019 Exploring extreme rainfall impacts on flow and turbidity dynamics in a steep, pristine and tropical volcanic catchment *Catena* **182** 104118
- [14] GUEYE M 2015 *Développement de charbon actif à partir de biomasses lignocellulosiques pour des applications dans le traitement de l'eau* (Institut International de l'Ingénierie de l'Eau et de l'Environnement (2))
- [15] Shafeeyan M S, Daud W M A W, Houshmand A and Shamiri A 2010 A review on surface modification of activated carbon for carbon dioxide adsorption *Journal of Analytical and Applied Pyrolysis* **89** 143–51
- [16] Onyango M S, Leswif T Y, Ochieng A, Kuchar D, Otieno F O and Matsuda H 2009 Breakthrough analysis for water defluoridation using surface-tailored zeolite in a fixed bed column *Industrial & Engineering Chemistry Research* **48** 931–7
- [17] Zhou Y, Davidson T A, Yao X, Zhang Y, Jeppesen E, de Souza J G, Wu H, Shi K and Qin B 2018 How autochthonous dissolved organic matter responds to eutrophication and climate warming: evidence from a cross-continental data analysis and experiments *Earth-Science Reviews* **185** 928–37
- [18] Adinata D, Daud W M A W and Aroua M K 2007 Production of carbon molecular sieves from palm shell based activated carbon by pore sizes modification with benzene for methane selective separation *Fuel processing technology* **88** 599–605
- [19] Daza L, Mendioroz S and Pajares J 1986 Preparation of Rh/active carbon catalysts by adsorption in organic media *Carbon* **24** 33–41
- [20] Danish M and Ahmad T 2018 A review on utilization of wood biomass as a sustainable precursor for activated carbon production and application *Renewable and Sustainable Energy Reviews* **87** 1–21
- [21] LU J 2005 Etude comparative sur les charbons actifs
- [22] Yorgun S and Yıldız D 2015 Slow pyrolysis of paulownia wood: Effects of pyrolysis parameters on product yields and bio-oil characterization *Journal of analytical and applied pyrolysis* **114** 68–78
- [23] Mamaní A, Sardella M F, Giménez M and Deiana C 2019 Highly microporous carbons from olive tree pruning: Optimization of chemical activation conditions *Journal of Environmental Chemical Engineering* **7** 102830
- [24] Sricharoenchaikul V, Pechyen C, Aht-ong D and Atong D 2008 Preparation and characterization of activated carbon from the pyrolysis of physic nut (*Jatropha curcas* L.) waste *Energy & Fuels* **22** 31–7
- [25] Meldrum B J and Rochester C H 1990 In situ infrared study of the surface oxidation of activated carbon dispersed in potassium bromide *Journal of the Chemical Society, Faraday Transactions* **86** 2997–3002
- [26] Sreńscek-Nazzal J and Kielbasa K 2019 Advances in modification of commercial activated carbon for enhancement of CO<sub>2</sub> capture *Applied Surface Science* **494** 137–51
- [27] Wang L, Tian C, Wang B, Wang R, Zhou W and Fu H 2008 Controllable synthesis of graphitic carbon nanostructures from ion-exchange resin-iron complex via solid-state pyrolysis process *Chemical communications* 5411–3
- [28] Cao F, Lian C, Yu J, Yang H and Lin S 2019 Study on the adsorption performance and competitive mechanism for heavy metal contaminants removal using novel multi-pore activated carbons derived from recyclable long-root *Eichhornia crassipes* *Bioresource technology* **276** 211–8
- [29] Ouyang T, Ye Y, Wu C, Xiao K and Liu Z 2019 Heterostructures Composed of N-Doped Carbon Nanotubes Encapsulating Cobalt and  $\beta$ -Mo<sub>2</sub>C Nanoparticles as Bifunctional Electrodes for Water Splitting *Angewandte Chemie International Edition* **58** 4923–8
- [30] Sun H, Liu S, Zhou G, Ang H M, Tadó M O and Wang S 2012 Reduced graphene oxide for catalytic oxidation of aqueous organic pollutants *ACS Applied Materials & Interfaces* **4** 5466–71
- [31] Liu L, Black R E, Cousens S, Mathers C, Lawn J E and Hogan D R 2015 Causes of child death: comparison of MCEE and GBD 2013 estimates *The Lancet* **385** 2461–2
- [32] Li L Y, Gong X and Abida O 2019 Waste-to-resources: Exploratory surface modification of sludge-based activated carbon by nitric acid for heavy metal adsorption *Waste Management* **87** 375–86
- [33] Altaweel A 2014 *Synthèse de nanostructures d'oxyde de cuivre par micro-post-décharge micro-ondes à pression atmosphérique* (France: Université de Lorraine)
- [34] Mthombeni N H, Mpenyana-Monyatsi L, Onyango M S and Momba M N 2012 Breakthrough analysis for water disinfection using silver nanoparticles coated resin beads in fixed-bed column *Journal of hazardous materials* **217** 133–40
- [35] Albayati T M and Kalash K R 2020 Polycyclic aromatic hydrocarbons adsorption from wastewater using different types of prepared mesoporous materials MCM-41 in batch and fixed bed column *Process Safety and Environmental Protection* **133** 124–36
- [36] Singha S and Sarkar U 2015 Analysis of the dynamics of a packed column using semi-empirical models: Case studies with the removal of hexavalent chromium from effluent wastewater *Korean Journal of Chemical Engineering* **32** 20–9
- [37] Sountharajah D P, Loganathan P, Kandasamy J and Vigneswaran S 2016 Column studies on the removal of dissolved organic carbon, turbidity and heavy metals from stormwater using granular activated carbon *Desalination and Water Treatment* **57** 5045–55
- [38] Torres-Lozada P, Amezcua-Marroquín C P, Agudelo-Martínez K D, Ortiz-Benítez N and Martínez-Ducua D S 2018 Evaluation of turbidity and dissolved organic matter removal through double filtration technology with activated carbon *Dyna* **85** 234–9